Smart Structures and Systems, *Vol. 23, No. 6 (2019) 565-577*
DOI: https://doi.org/10.12989/sss.2019.23.6.565

Multi-mode cable vibration control using MR damper based on nonlinear modeling

H.W. Huang*[1,2], T.T. Liu[3a] and L.M. Sun[1,2b]

[1]*State Key Laboratory for Disaster Reduction in Civil Engineering, Tongji University, 1239 Siping Road, Shanghai, China*
[2]*Department of Bridge Engineering, Tongji University, 1239 Siping Road, Shanghai, China*
[3]*Hunan Provincial Communications Planning, Survey & Design Institute Co., Ltd., Changsha 410200, China*

(Received July 12, 2016, Revised January 12, 2019, Accepted January 25, 2019)

Abstract. One of the most effective countermeasures for mitigating cable vibration is to install mechanical dampers near the anchorage of the cable. Most of the dampers used in the field are so-called passive dampers where their parameters cannot be changed once designed. The parameters of passive dampers are usually determined based on the optimal damper force obtained from the universal design curve for linear dampers, which will provide a maximum additional damping for the cable. As the optimal damper force is chosen based on a predetermined principal vibration mode, passive dampers will be most effective if cable undergoes single-mode vibration where the vibration mode is the same as the principal mode used in the design. However, in the actual engineering practice, multi-mode vibrations are often observed for cables. Therefore, it is desirable to have dampers that can suppress different modes of cable vibrations simultaneously. In this paper, MR dampers are proposed for controlling multi-mode cable vibrations, because of its ability to change parameters and its adaptability of active control without inquiring large power resources. Although the highly nonlinear feature of the MR material leads to a relatively complex representation of its mathematical model, effective control strategies can still be derived for suppressing multi-mode cable vibrations based on nonlinear modelling, as proposed in this paper. Firstly, the nonlinear Bouc-wen model is employed to accurately portray the salient characteristics of the MR damper. Then, the desired optimal damper force is determined from the universal design curve of friction dampers. Finally, the input voltage (current) of MR damper corresponding to the desired optimal damper force is calculated from the nonlinear Bouc-wen model of the damper using a piecewise linear interpolation scheme. Numerical simulations are carried out to validate the effectiveness of the proposed control algorithm for mitigating multi-mode cable vibrations induced by different external excitations.

Keywords: stay cable; multi-mode vibration; semi-active control; MR damper;optimal friction damper force

1. Introduction

Installation of mechanical dampers near the anchorages of cables have been proved to be one of the most effective countermeasures for vibration mitigation of stay cables in various cable-stayed bridges (ex., Main and Jones 2002a, b). Most of the dampers used in the field are so-called passive dampers where their parameters cannot be changed once designed. The parameters of passive dampers are usually determined based on the optimal damper force obtained from the universal design curve for linear dampers (Pacheco *et al*. 1993), which will provide a maximum additional damping for the cable. As the optimal damper force is chosen based on a predetermined principal vibration mode, passive dampers will be most effective if cable undergoes single-mode vibration where the vibration mode is the same as the principal mode used in the design (ex., Tabatabai and Mehrabi 2000). However, in the actual engineering practice, multi-mode vibrations are often observed for cables. Therefore, it is desirable to have dampers that can suppress different modes of cable vibrations simultaneously.

Wang *et al*. (2005) developed a new method for optimal damper size design to achieve multi-mode cable vibration control by means of an active control algorithm. Ying *et al*. (2007) studied multi-mode cable vibration and the influences of the cable structure parameters and control factors on the parametrically excited instability of a semi-actively controlled cable. Weber *et al*. (2009) presented a systematic and applicable design procedure for linear viscous dampers targeting multiple cable modes. Huang *et al*. (2012) explored the possibility of using MR damper for mitigating multi-mode cable vibrations where the parameters of MR damper was tuned based on linear optimal damper force and can be changed automatically when the principal modes in actual cable vibrations shift. Duan *et al*. (2019a, b) derived the general design formulas for cable vibration control using MR dampers (Chen *et al*. 2004, Duan *et al*. 2005, Duan *et al*. 2006, Or *et al*. 2008). Duan *et al*. (2018) presented a hybrid simulation method to evaluate the enhanced cable damping due to installation of

*Corresponding author, Professor
E-mail: hongweih@tongji.edu.cn
[a] Ph.D.
E-mail: 91tingliu@tongji.edu.cn
[b] Ph.D.
E-mail: lmsun@tongji.edu.cn

ISSN: 1738-1584 (Print), 1738-1991 (Online)

linear viscous dampers. Lu *et al.* (2017) investigated viscous inertial mass damper (VIMD) for mitigating cable vibration and showed better effectiveness than linear viscous damper. The above studies were carried out based on theories for linear dampers. However, it was shown that nonlinear dampers, especially friction dampers, can provide larger maximum additional damping to the cable (ex., Main and Jones 2002b, Weber *et al*. 2010, Wang and Sun 2013), and therefore, the nonlinear features of MR damper should be further utilized.

In this paper, continuous studies will be carried out to investigate the performance of MR dampers in controlling multi-mode cable vibrations. Effective control strategies will be derived based on the universal design curve of friction dampers, where the optimal control force will be obtained through the relation between the damper force and the amplitude of vibration at damper location derived by Wang and Sun (2013). The physical behavior of MR damper will be portraited using the modified Bouc-Wen model (Spencer *et al*. 1997) instead of the bilinear model (Huang *et al*. 2012, 2015), in order to minimize the deviation of modelling, because the modified Bouc-Wen model has been proved to be most accurate in describing the energy dissipating mechanism of MR damper even in the region of small velocity (Spencer *et al*. 1997). Finally, the input voltage (current) of MR damper corresponding to the desired optimal damper force is calculated from the nonlinear Bouc-wen model of the damper using a piecewise linear interpolation scheme (Weber 2013). A series of numerical simulations are carried out to validate the effectiveness of the proposed control algorithm for mitigating multi-mode cable vibrations induced by different loading scenarios such as sinusoidal excitations, white noise excitations and wind loads.

2. Optimal control algorithm for cable vibration using MR damper

In order to derive the optimal control algorithm for cable-MR damper system, the state-space representation of the cable is first established by adapting equations given in Johnson *et al*. (2007), then the desired damper force is determined from the universal design curve of nonlinear dampers derived by Wang and Sun (2013), and finally the corresponding input voltage (current) of MR damper is calculated using a piecewise linear interpolation scheme (Weber 2013) on the desired damper force based on the nonlinear Bouc-Wen model of MR damper (Spencer *et al*. 1997). The detail derivations are described in the following

2.1 Establish state-space representation of cable

A typical cable-MR damper system can be shown by Fig. 1, where the length of the cable is *l*, the mass per unit length is m, the uniform inherent damping ofthe cable is *c* and the cable tension is T. The damper is located at a distance of a from the anchorage of the cable with the damper force denoted by F_d. It is assumed that the cable force is unchanged under linear oscillations, the bending

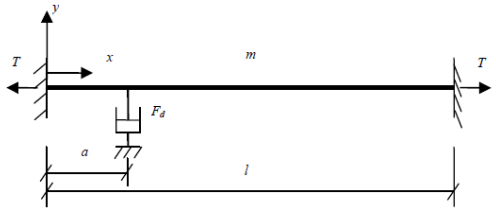

Fig. 1 Cable-MR damper system

stiffness is negligible, and the effects of sag and inclination are ignored.

The motion of the above cable in the linear range can be described by the following partial differential equation

$$m\frac{\partial^2 y}{\partial t^2}+c\frac{\partial y}{\partial t}-T\frac{\partial^2 y}{\partial x^2}=F(x,t)F_d\delta(x-a) \tag{1}$$

where $y(x,t)$ is the transverse deflection of the cable; $F(x,t)$ is the distributed load on the cable; F_d is the transverse damper force at $x=a$ location; and $\delta(\cdot)$ is the Dirac delta function.

The boundary conditions associated with the above equation of motion are

$$y(0,t)=y(l,t)=0 \tag{2}$$

The transverse deflection can be approximated by a finite series in the form (Pacheco *et al*. 1993) of

$$\mathrm{y}(x,t)=\sum_{i=1}^{n}q_i(t)\varphi_i(x) \tag{3}$$

where *n* is the number of degree-of-freedoms, $q_i(t)$ is the generalized displacements and $\varphi_i(x)$ is the set of shape functions which is selected to be sinusoidal functions as

$$\varphi_i(x)=\sin(\pi ix/l) \tag{4}$$

As $\varphi_i(x)$ is proportional to the i th undamped mode shape of the cable, Eq.(1) can be transformed to an equation of motion in terms of the generalized displacements by standard Galerkin method, as given in Eq. (5), where Eq. (3) is substituted into Eq. (1), multiplied by $\varphi_i(x)$ and integrated over the length (Johnson *et al*. 2007)

$$M\ddot{q}+C\dot{q}+Kq=F_q(t)+\varphi(a)F_d(t) \tag{5}$$

where

$$m_{ij}=m\int_0^l\frac{\sin\pi ix}{l}\frac{\sin\pi jx}{l}dx=\frac{ml}{2}\delta_{ij} \tag{6}$$

$$k_{ij}=-T\int_0^l\frac{\sin\pi ix}{l}\left(\frac{\sin\pi jx}{l}\right)^{''}dx=\frac{T\pi^2i^2}{2l}\delta_{ij} \tag{7}$$

$$F_{qi}(t)=\int_0^l F(x,t)\sin(i\pi x/l)dx \tag{8}$$

$$\varphi(a)=\sin\left(i\pi a/l\right) \tag{9}$$

As these sinusoidal shape functions are mutually orthogonal to each other, the transformed mass $M=[m_{ij}]$ and stiffness $K=[k_{ij}]$ matrices are diagonal. Finally, the state-space representation of the cable can be obtained by introducing a state vector $x(t)=\begin{Bmatrix} q(t) \\ \dot{q}(t) \end{Bmatrix}_{2n\times 1}$ and further transforming Eq. (5) as

$$\begin{cases} \dot{x}=Ax+Bu \\ y=Cx+Du \end{cases} \tag{10}$$

where

$$A=\begin{bmatrix} 0 & I \\ -M^{-1}K & 0 \end{bmatrix},\quad B=\begin{bmatrix} 0 \\ M^{-1}Bss \end{bmatrix},\quad C=\begin{bmatrix} I & 0 \\ 0 & I \end{bmatrix},$$

$$D=\begin{bmatrix} 0 \\ 0 \end{bmatrix},\quad u=\begin{bmatrix} F(t) \\ F_d(t) \end{bmatrix},\quad Bss=\begin{bmatrix} Ds & Bs \end{bmatrix}$$

Eqs. (1)-(10) are adapted from (Johnson *et al*. 2007).

2.2 Determine desired damper force

As discussed by many researchers, the mechanical model of MR damper is highly nonlinear and the damper force varies with the amplitude of vibration (displacement) in a way similar to that of a friction damper which is a highly nonlinear damper, except for the region where the velocity is small. Hence, the desired optimal damper force can be approximated by the universal design curve of friction damper (shown in Fig. 2) derived by Wang and Sun (2013), which is expressed by the following equation

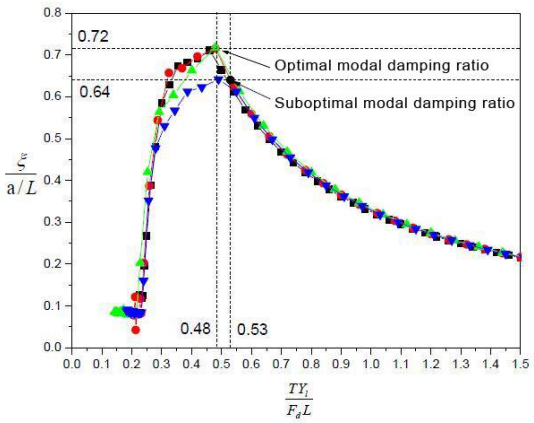

Fig. 2 Universal design curve of friction damper

$$F_{des}=-\mathrm{sgn}(\dot{y}_d)\frac{T}{a}Y_d \tag{11}$$

where T is the cable tension, and Y_d and $\dot{y}_d$ are the amplitude and velocity of cable vibration at damper location $x=a$ respectively.

2.3 Calculate corresponding input voltage (or Current) of MR damper

2.3.1 Modified Bouc-Wen model of MR damper

It has been proved by Spencer *et al*. (1997) that the modified Bouc-Wen model shown in Fig. 3 portraits the physical behavior of MR damper more accurately than other models, and therefore, it will be used in this paper for deriving the direct relations between damper force and input voltage (or current) of the MR damper.

As proposed in Spencer *et al*. (1997), the governing equations are given by

$$c_1\dot{y}=\alpha z+k_0(x-y)+c_0(\dot{x}-\dot{y}) \tag{12}$$

$$\dot{z}=-\gamma|\dot{x}-\dot{y}||z|^{n-1}-\beta(\dot{x}-\dot{y})|z|^n+A(\dot{x}-\dot{y}) \tag{13}$$

$$F=\alpha z+c_0(\dot{x}-\dot{y})+k_0(x-y)+k_1(x-x_0) \tag{14}$$

where z is the evolutionary variable.

To simulate the magnetic field generated by MR fluid, the following parameters are expressed as functions of applied voltage (or current) u

$$\alpha=\alpha(u)=\alpha_a+\alpha_b u \tag{15}$$

$$c_1=c_1(u)=c_{1a}+c_{1b}u \tag{16}$$

$$c_0=c_0(u)=c_{0a}+c_{0b}u \tag{17}$$

Then, a first-order filter is used to represent the dynamic equilibrium in the MR fluid as

$$\dot{u}=-\eta(u-v) \tag{18}$$

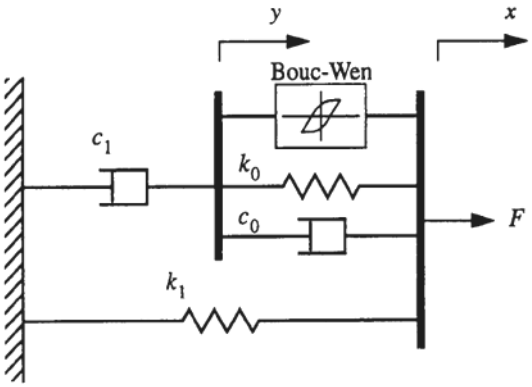

Fig. 3 Modified Bouc-Wen Model of MR Damper

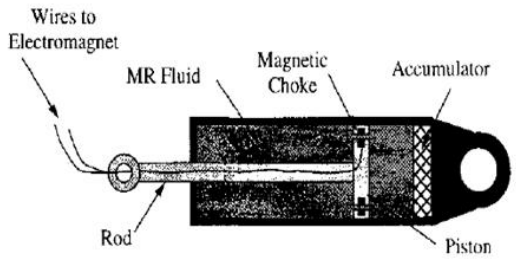

Fig. 4 Schematic of MR Damper

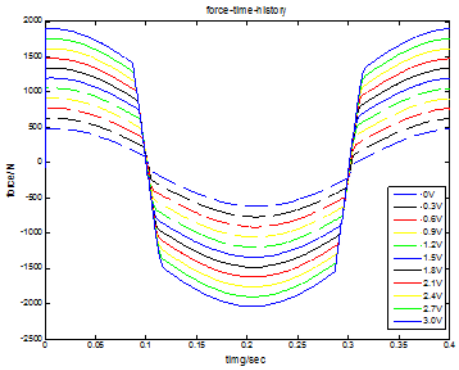

Fig. 5 Damper force under 2.5 Hz sinusoidal vibration with amplitude of 1.5 cm

Table 1 Parameters of Generalized Bouc-Wen Model

Parameter	Value	Parameter	Value
c_{0a}	21.0N s/cm	α_a	140N/cm
c_{0b}	3.50N s/$cm\cdot V$	α_b	695 $N/cm\cdot V$
k_0	46.9 N/cm	γ	363 cm^{-2}
c_{1a}	283 N s/cm	β	363 cm^{-2}
c_{1b}	2.95 N s/$cm\cdot V$	A	301
k_1	5.0 N/cm	n	2
x_0	14.3 cm	η	190S^{-1}

where v is the voltage (or current) applied to the current driver. Finally, the optimal values of a total of 14 parameters (c_{0a}, c_{0b}, k_0, c_{1a}, c_{1b}, k_1, x_0, α_a, α_b, γ, β, A, n, η) are determined (as summarized in Table 1) for the prototype MR damper(Spencer *et al*. 1997) shown in Fig. 4, which is a small-scale MR damper with a maximum damping force of 3000N.

The damper is 21.5 cm long in its extended position and has a stroke of $\pm$2.5 cm. This prototype is very similar to the actual MR damper installed on stay cables of cable-stayed bridges and therefore, will be used in the following simulation studies.

The damper force is computed based on the displacement at damper location and the input voltage of the MR damper. The response of the damper under a 2.5 Hz sinusoid vibration with an amplitude of 1.5 cm is shown in Fig. 5 with 11 constant voltage levels from 0 to 3V with an internal of 0.3 V. It can be seen that, at 0 V, the MR damper primarily exhibits the characteristics of a purely linear viscous device. However, as the voltage increases, the damper force increases and produces a behavior of a plastic material in parallel with a linear viscous damper. Also, it is notice that the damper force increases approximately linearly with the applied voltage for in the range of 0 to 3V.

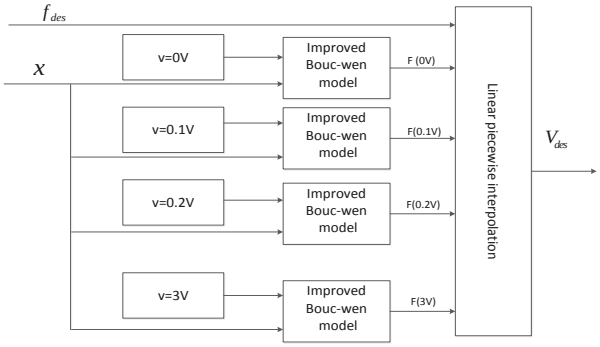

Fig. 6 Block diagram of piecewise linear interpolation scheme

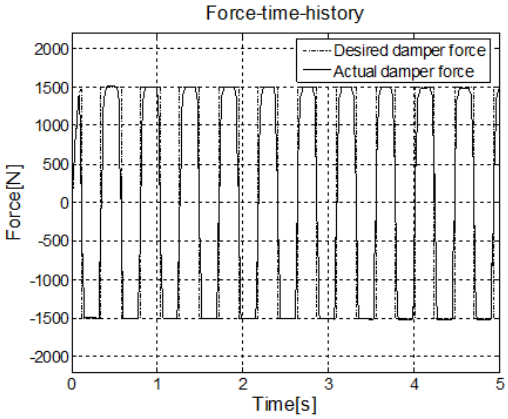

Fig. 7 Comparison of actual damper force and desired control force

2.3.2 Piecewise linear interpolation scheme

Although the modified Bouc-Wen model describes well the highly nonlinear feature of MR damper, it has difficulties forming a simple relationship between the damper force and the input voltage applied to the current driver. In this paper, a piecewise linear interpolation scheme (Weber 2013) based on the modified Bouc-Wen model mentioned above is used to determine the desired input voltage of MR damper corresponding to the desired optimal

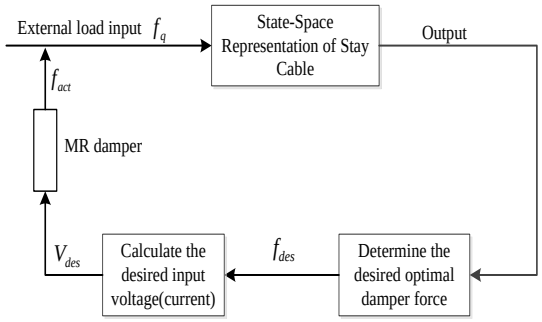

Fig. 8 Block diagram of the semi-active control system

damper force. Firstly, a series of MR damper force levels are computed using the modified Bouc-Wen model by inputting different constant voltages and with actual MR damper displacement and velocity. Then, the desired optimal damper force is obtained from Eq. (11) and the universal design curve plotted in Fig. 2. Finally, the desired input voltage is obtained by interpolating the desired optimal damper force between the predetermined damper force levels using a piecewise linear interpolation scheme as shown in Fig. 6.

The accuracy and efficiency of the piecewise linear interpolation scheme is validated by simulation (shown in Fig. 7). The actual damper force approximated through the piecewise linear interpolation scheme differs only slightly from the desired damper force.

The optimal control strategy of cable vibration using MR damper can be illustrated by the flow chart shown in Fig. 8 and summarized as follows. Because when the input voltage (current) of MR damper increases, the energy dissipation behavior of MR damper gets closer to a Friction damper, Eq. (11) will be used to approximate the desired optimal damper force.

(1) The instant displacement at damper location Y_d, is determined.

(2) The desired MR damper force is estimated using Eq. (11) by substituting values of Y_d and $\dot{y}_d$ with given parameters T and a of the selected cable.

(3) The corresponding input voltage of MR damper is obtained by interpolating the desired optimal damper force between the predetermined damper force levels using the proposed piecewise linear interpolation scheme.

(4) The actual damper force is computed from the modified Bouc-Wen model of MR damper using the actual input voltage obtained in step (3) and the displacement at damper location determined in step (1).

3. Multi-mode cable vibration control

Numerical studies were carried out using SIMULINK of Matlab. An 80 m long stay cable was established with parameters listed in Table 2. In order to formulate the equation of motion, the cable was divided into 200 elements with equal length and the corresponding system mass matrix *M* and stiffness matrix *K* in Eq. (5) were established, from which the modal frequencies and mode shapes can be obtained.

In order to verify the effectiveness and efficiency of the proposed control scheme of using MR damper for suppressing multi-mode cable vibration, different loading scenarios will be considered in numerical studies. Firstly, mixes of lower modes vibration will be generated by applying sinusoidal excitations to the cable. Then, white noise excitation will be used to demonstrate a more general case of cable vibration where higher modes are included. Finally, a typical type of wind induced vibration will be excited to illustrate the case of common cable vibration phenomenon observed in the field. All the displacements were measured in meter and time measured in seconds.

3.1 Sinusoidal excitation

Three different distributed sinusoidal loads were applied simultaneously to the cable, each has frequency coincide with the first, second and third natural frequency of the cable respectively and distributed shape matches with the corresponding first, second and third mode shape of the cable respectively, such that a mixes of the first three modes of vibration were generated. In order to study the effect of the shift of principal vibration mode, three different loading cases were considered and the simulation time of each case was 10 seconds.

Case 1: The first mode was selected as the principal vibration mode, and thus, the amplitude of the distribute shape corresponding to this mode was assumed to be double of other modes and the total distributed load is in the form of $F(x,t)=2\sin(\pi x/l)\sin(\omega_1 t)+\sin(2\pi x/l)\sin(\omega_2 t)+\sin(3\pi x/l)\sin(\omega_3 t)$. The time histories and power spectrum of displacement responses at damper location and the mid-span, with and without MR damper, were shown in Fig. 9, where dash lines represented cable vibrations without damper, while solid lines demonstrated vibrations with damper. The decay ratio which is defined as the reduction of the peak value of the power spectrum of displacement responses were calculated and shown in Table 3, for the purpose of comparing the control effect on different vibration modes.

Case 2: The second mode was selected as the principal vibration mode, where the amplitude of the distribute shape corresponding to this mode was assumed to be double of other modes and the total distributed load is in the form of $F(x,t)=\sin(\pi x/l)\sin(\omega_1 t)+2\sin(2\pi x/l)\sin(\omega_2 t)+\sin(3\pi x/l)\sin(\omega_3 t)$

The time histories and power spectrum of displacement responses at damper location and the one fourth of the cable length were shown in Fig. 10, with dash and solid lines representing cable vibrations without and with damper respectively. The comparison of the decay ratio of the power spectrum of displacement responses for different vibration modes were shown in Table 4.

Case 3: The third mode was selected as the principal vibration mode, where the amplitude of the distribute shape corresponding to this mode was assumed to be the double of other modes and total distributed load is in the form of $F(x,t)=\sin(\pi x/l)\sin(\omega_1 t)+\sin(2\pi x/l)\sin(\omega_2 t)+2\sin(3\pi x/l)\sin(\omega_3 t)$.

The time histories and power spectrum of displacement responses at damper location and the one sixth of the cable length were shown in Fig. 11, with dash and solid lines representing cable vibrations without and with damper respectively. The comparison of the decay ratio of the power spectrum of displacement responses for different vibration modes were shown in Table 5.

Table 2 Main parameters of cable

L (m)	*T* (kN)	*m* (kg/m)	*a* (m)	*c*(N·s/m)
80	1226	10	3.2	0.22

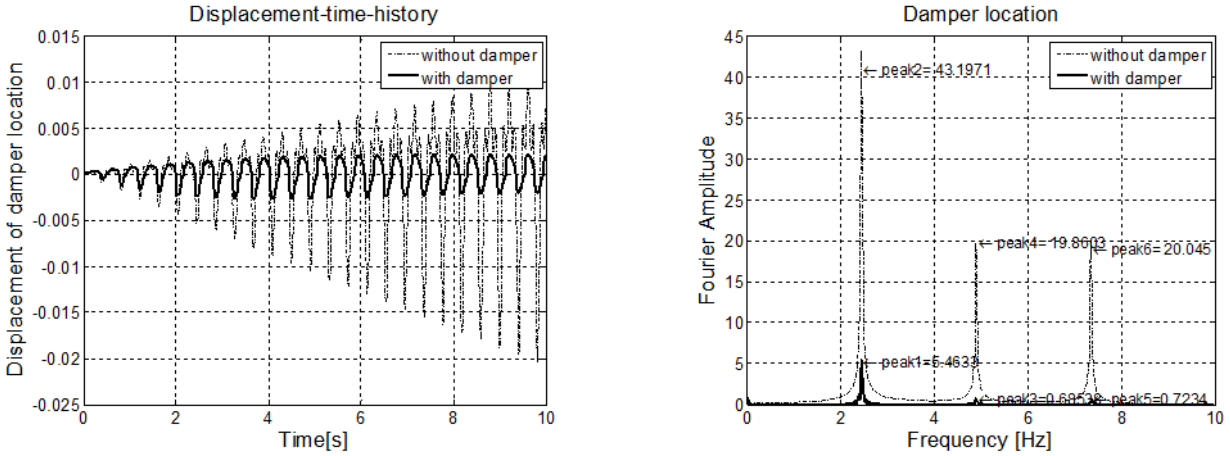

(a) at damper location

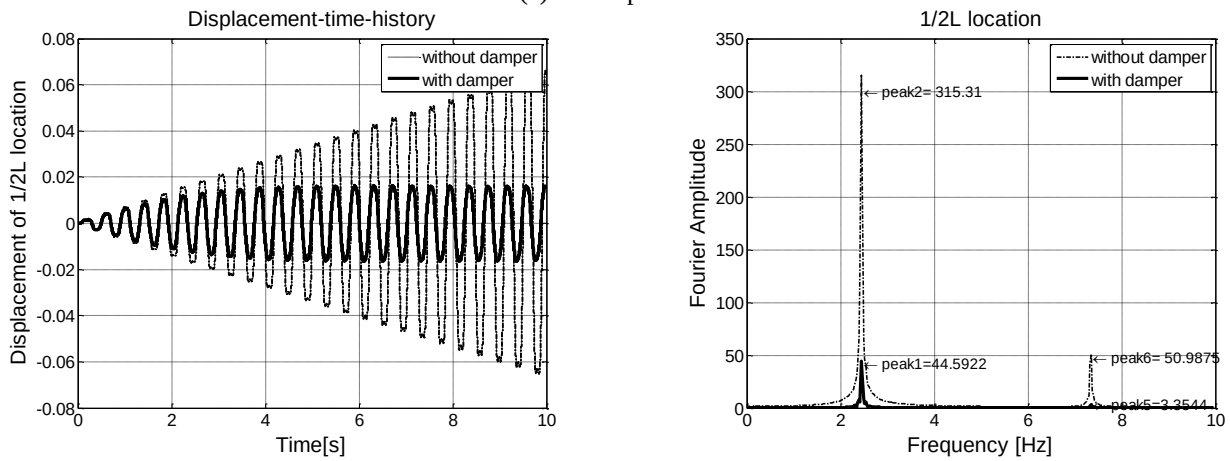

(b) at mid-span

Fig. 9 Time history and power spectrum of displacement response (case 1)

Table 3 Comparison of the decay ratio of the power spectrum of displacement responses (case 1)

Location	Control measure	First mode		Second mode		Third mode	
		p	Decay ratio ζ	p	Decay ratio ζ	p	Decay ratio ζ
Damper location	w/o D	43.1971		19.8603		20.0450	
	w D	5.4633	87.35%	0.6854	96.55%	0.7234	96.39%
Mid-span	w/o D	315.310				50.9875	
	w D	44.5922	85.86%			3.3544	93.42%

Note: "p" *means* "*peak value of power spectrum*"; "*w/o D*" *means* "*without damper*"; "*w D*" *means* "*with damper*".

It can be observed from Figs. 9-11 that for different loading cases, cable vibrations were well suppressed with the installation of MR damper, and also, not only the principal vibration mode, every other mode of vibration was significantly reduced. Further, Tables 3-5 illustrated that the energy in higher mode dissipated faster because higher mode has more cycles of vibration within the same simulation time period and consequently the damper went through more cycles of energy dissipation.

The performance of the MR damper can also be demonstrated by comparing the RMS values of displacement responses, before and after installing the optimally tuned MR damper, as summarized in Table 6. Again, it shows that with the installation of MR damper, the vibration of the cable was mitigated substantially. The reduction rate of the RMS value in different loading cases at damper location is about 73%, and at the location of maximum amplitude of vibration it is around 66% for case 1 (mid-span), 66% for case 2 (1/4*L*) and 68% for case 3 (1/6*L*).

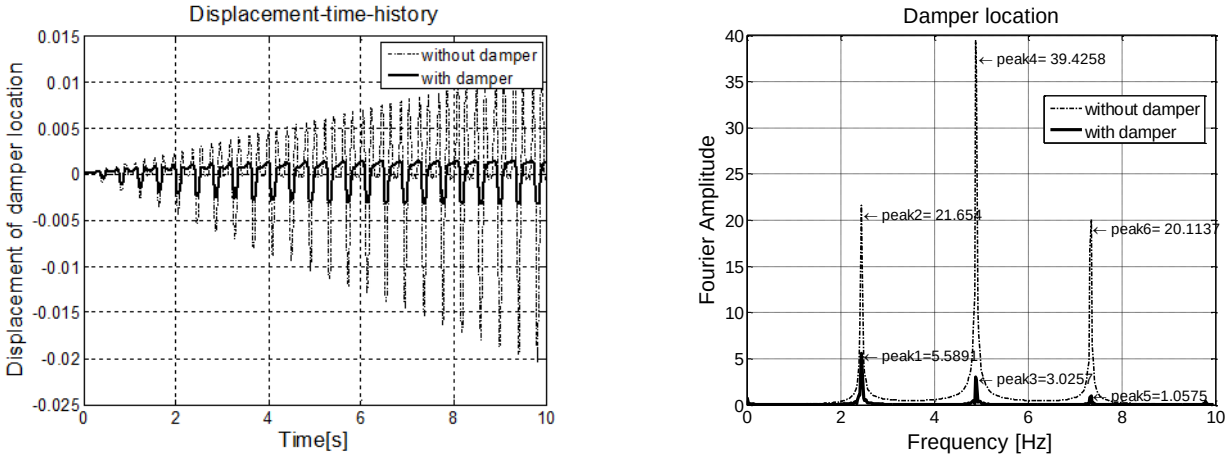

(a) at damper location

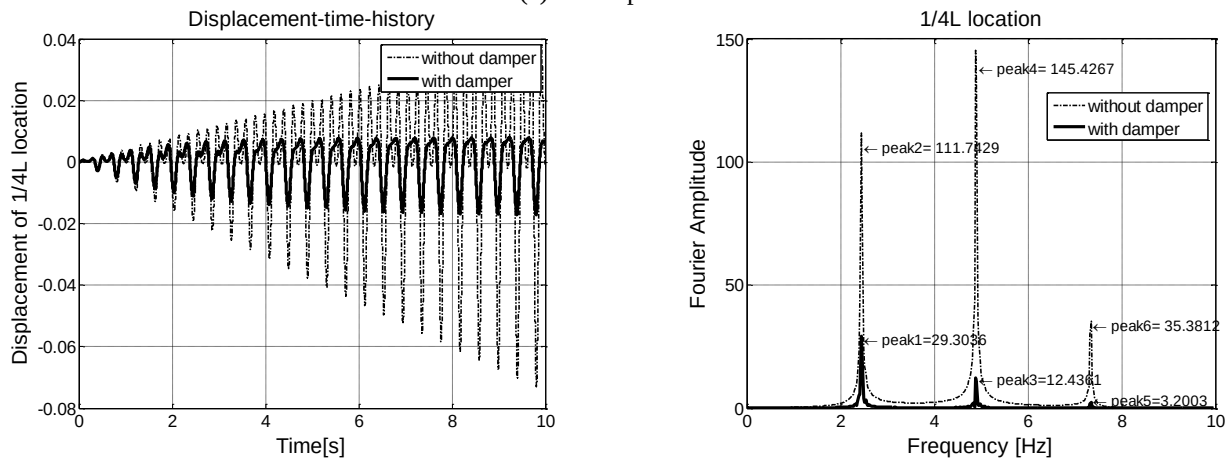

(b) at mid-span

Fig. 10 Time history and power spectrum of displacement response (case 2)

Table 4 Comparison of the decay ratio of the power spectrum of displacement responses (case 2)

Location	Control measure	First mode		Second mode		Third mode	
		p	Decay ratio ζ	p	Decay ratio ζ	p	Decay ratio ζ
Damper location	w/o D	21.6540		39.4258		20.1137	
	w D	5.5891	74.19%	3.0257	92.33%	1.0575	94.74%
1/4L location	w/o D	111.742		145.427		35.3812	
	w D	29.3036	73.78%	12.4361	91.45%	3.2003	90.95%

Note: "*p*" *means* "*peak value of power spectrum*"; "*w/o D*" *means* "*without damper*"; "*w D" means* "*with damper*".

Table 5 Comparison of the decay ratio of the power spectrum of displacement responses (case 3)

Location	Control measure	First mode		Second mode		Third mode	
		p	Decay ratio ζ	p	Decay ratio ζ	p	Decay ratio ζ
Damper lo cation	w/o D	21.5627		19.7434		40.2279	
	w D	4.4923	79.17%	2.1625	89.05%	1.3312	96.69%
1/6L location	w/o D	78.7597		63.0573		100.334	
	w D	16.7716	78.71%	6.8945	89.07%	4.7219	95.29%

Note: "*p*" *means* "*peak value of power spectrum*"; "*w/o D*" *means* "*without damper*"; "*w D" means* "*with damper*".

Table 6 Comparison of the RMS value of displacement responses under different loading cases

Location	Control measure	Case 1		Case 2		Case 3	
		σ_{rms}	Reduction rate	σ_{rms}	Reduction rate	σ_{rms}	Reduction rate
Damper location	w/o D	5.2893		5.2758		5.2230	
	w D	1.4494	72.60%	1.4336	72.83%	1.3463	74.22%
Location of maximum amplitude	w/o D	32.1376		19.8134		14.8886	
	w D	10.9341	65.98%	6.8716	66.32%	4.7579	68.04%

Note: "*p*" *means* "*peak value of power spectrum*"; "*w/o D*" *means* "*without damper*"; "*w D" means* "*with damper*".

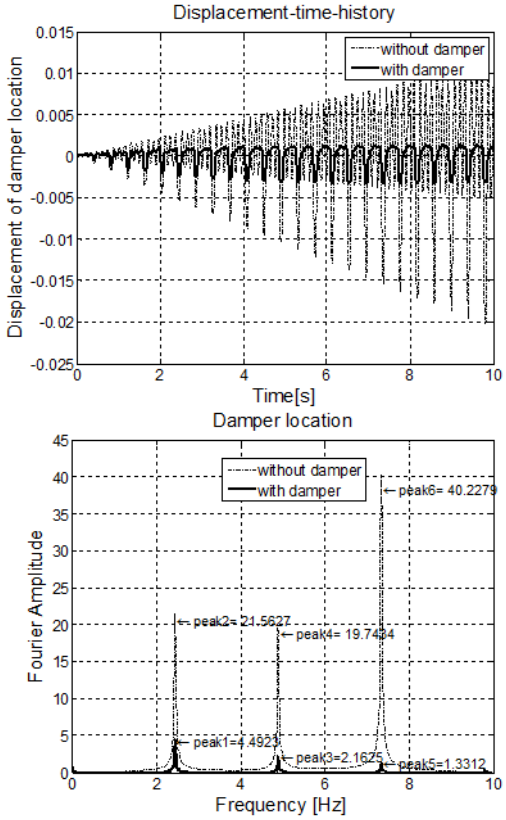

(a) at damper location

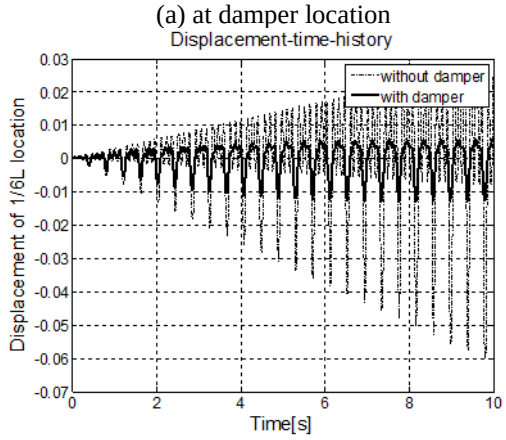

Continued-

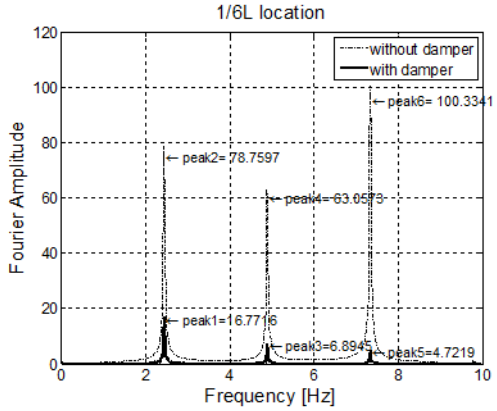

(b) at 1/6L location

Fig. 11 Time history and power spectrum of displacement response (case 3)

All these results proved that using the proposed control algorithm where MR damper was tuned to the optimal friction damper force, multi modes of cable vibrations can be controlled at the same time. Because the damper worked as a friction damper, its effectiveness did not depend on the mode of vibration but rather on the amplitude of vibration.

3.2 White noise excitation

In the previous session, the effectiveness of the proposed control algorithm for suppressing multi-mode cable vibration was verified using cases of lower modes of vibrations, while in this session a more general case was studied where higher modes of vibrations were induced by applying a Gaussian white noise excitation to the cable. Two different loading cases were considered. In case 1, the white noise excitation was applied at position $L/10$ of the cable and in case 2 the same form of excitation was applied at $L/20$ of the cable. In both cases, multi modes of cable vibrations were excited and the simulation time was 10 seconds.

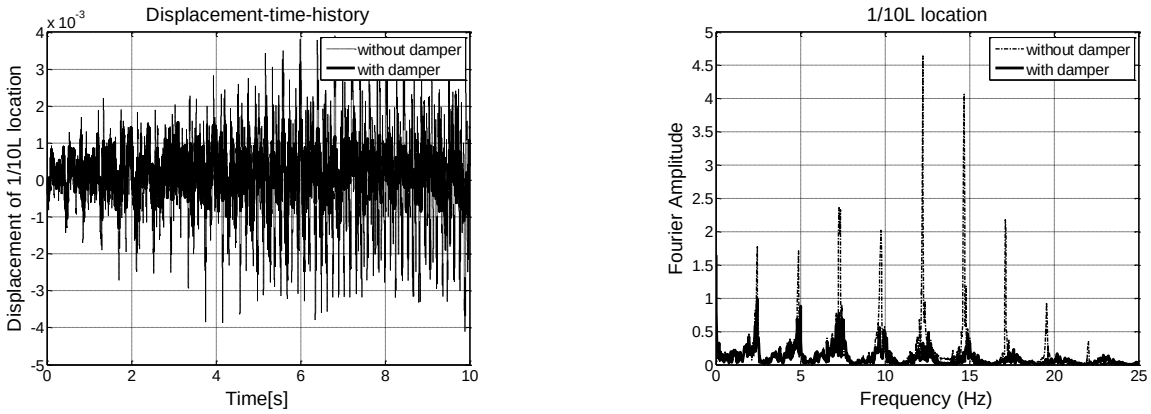

(a) at damper location (b) at 1/10*L* location

Fig. 12 Time history and power spectrum of displacement response with white noise excitation applied at 1/10L location

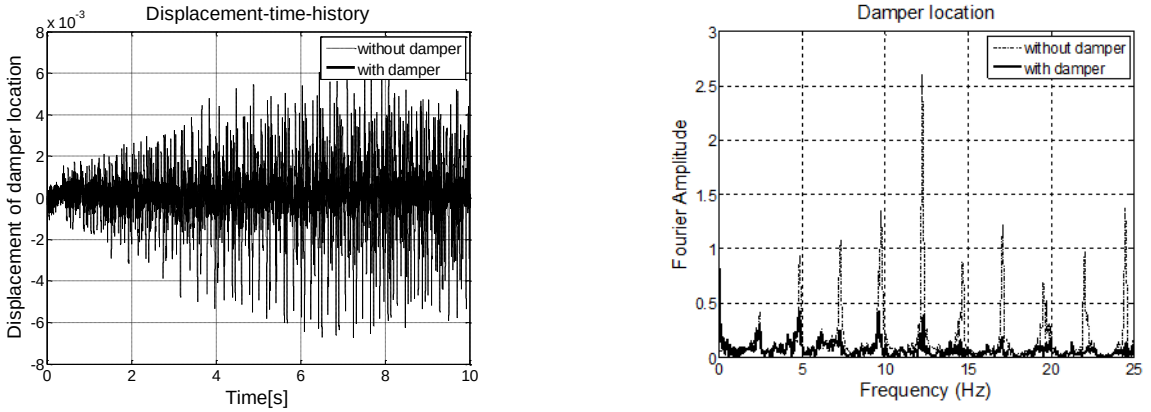

(a) at damper location

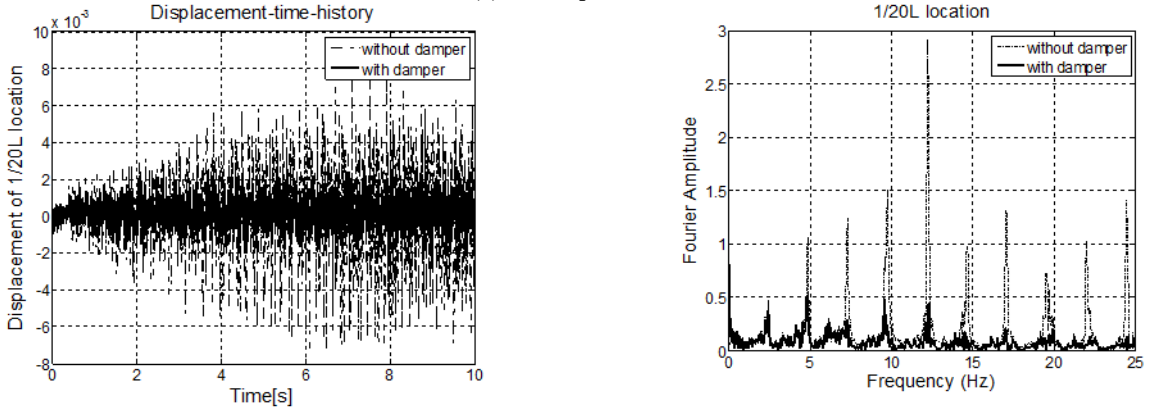

(b) at 1/20*L* location

Fig. 13 Time history and power spectrum of displacement response with white noise excitation applied at 1/20L location

The time history of the displacement responses at the damper location and at the excitation point, with and without the installation of MR damper, were plotted in Fig. 12, and the corresponding power spectrums were shown in Fig. 13. In both figures, the dashed line and the solid line represented the measured data before and after installing MR damper respectively. It can be seen from Figs. 12 and13 that for each loading case, the vibration energy of each vibration mode of the cable was significantly reduced by MR damper which was tuned to the optimal friction damper force using the proposed control strategy. The comparison of the RMS value of the displacement response at different locations, with and without MR damper, was shown in Table 7. It is also noted that with the installed optimally tuned MR damper, the vibration of the cable was suppressed substantially. Besides, the reduction rate at each location under loading case 1 is slightly higher than that under loading case 2, which showed that the effectiveness of MR damper is more apparent when the excitation point is closer to the damper location.

Table 7 Comparison of the RMS value of the displacement responses under different loading cases

Excited location	Control measure	Damper location		1/2L location		Excited point	
		σ_{rms}	Reduction rate	σ_{rms}	Reduction rate	σ_{rms}	Reduction rate
L/10	w/o D	1.1504	--	1.5583	--	1.5596	--
	w D	0.3114	72.93	0.7384	52.61	0.5583	64.20
L/20	w/o D	0.4854	--	0.8575	--	0.5986	--
	w D	1.9459	75.05	2.2629	62.11	2.0677	71.05

Note: "*p*" *means* "*peak value of power spectrum*"; "*w/o D*" *means* "*without damper*"; "*w D" means* "*with damper*".

The above results indicated that the proposed optimal control strategy using MR damper effectively mitigated multi-mode cable vibrations under general loading conditions where both lower and higher vibration modes were induced.

3.3 Wind induced vibration

In this session, a typical type of wind induced vibration was studied, where fluctuating wind field was generated using the method of weighted amplitude wave superposition (WAWS) and Kaimal spectrum as proposed in Liu *et al.* (2013). The total time of simulation was 60 seconds.

3.3.1 Generation of wind load

The horizontal and vertical wind velocities obtained using WAWS can be transferred to the buffeting force of the drag and lift parts respectively, by substituting into Eqs. (19) and (20)

$$D_s = \frac{1}{2}\rho U^2 D\left\{2C_D(\gamma)\frac{u(t)}{U} + C_D'(\gamma)\frac{w(t)}{U}\right\} \quad (19)$$

$$L_s = \frac{1}{2}\rho U^2 D\left\{2C_L(\gamma)\frac{u(t)}{U} + (C_L'(\gamma) + C_D)\frac{w(t)}{U}\right\} \quad (20)$$

where D_S is the buffeting force of the drag part and L_S is the buffeting force of the lift part; ρ is the air density of value 1.2kg/m^3; U is the average wind speed; $u(t)$ and $w(t)$ are the time-history of wind speed in horizontal and vertical direction respectively, obtained using WAWS; D is the characteristic width; γ is the wind attack angle; C_D and C_L are the drag and lift coefficient; C_D' and C_L' are the derivatives of C_D and C_L with respect to γ, whose suggested values for civil engineering application are shown in Table 8.

Table 8 Drag and lift coefficients of the cable

C_D	C_L	C_D'	C_L'
0.723	-0.122	0	0

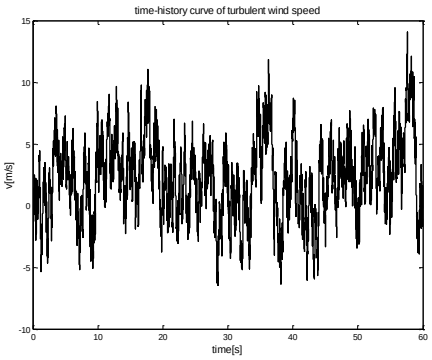

(a) horizontal turbulent wind speed

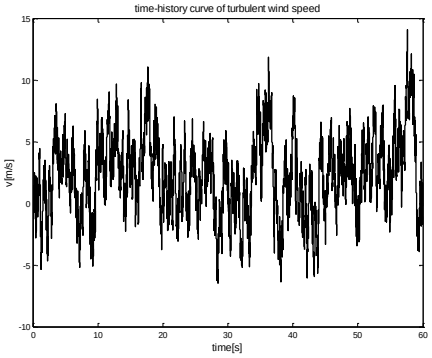

(b) vertical turbulent wind speed

Fig. 14 Time-history sample curves of turbulent wind speeds at the midpoint of the cable

The resultant buffeting force acting perpendicular to the cable can be obtained by substituting the drag and lift forces given in Eqs. (19) and (20) into Eq. (21), and the modal wind load can be obtained by substituting Eq. (21) into Eq. (22), in order to formulate the state space representation of the equation of motion of the cable in carrying out the control algorithm.

$$F(x,t) = L_s\cos\alpha - D_s\sin\alpha \quad (21)$$

$$f_q(i) = \sum_{j=1}^{n_p} F(x_j,t)\sin(i\pi\frac{j\Delta x}{L})\Delta x \qquad i = 1,2,\cdots,n_k \quad (22)$$

where n_k is the mode number; n_p is the sampling number; Δx is the wind load sampling interval.

The cable is divided to 80 sections, each of which is 1m long, and 79 wind velocity points were obtained, neglecting two endpoints. The time-history sample curves of horizontal and vertical turbulent wind speeds at the midpoint of the cable is shown in Fig. 14, and a comparison between the simulated and the target spectrums in both horizontal and vertical directions is given in Fig. 15. The results indicated that WAWS is an effective and accurate way of simulating the turbulent wind field numerically and is reliable to be used to generate wind induced vibration in this session.

3.3.2 Wind induced vibration

Applying the modal wind load given in Eq. (22) along the cable, wind induced vibration was generated subsequently.

The time histories and power spectrums of the displacement responses at damper location, mid-span and 1/4*L* of the cable, with and without MR damper, were plotted in Fig. 16, where the dashed line and solid line represented the uncontrolled and controlled systems respectively. The displacement time history showed that the vibration of cable could be effectively suppressed using MR damper with the proposed control algorithm. The corresponding power spectrums indicated that the vibration energy of the cable is much reduced, and the cable was excited to vibrate in multi modes at the damper location, while the primary vibration mode at both mid-span and 1/4*L* locations was the first mode.

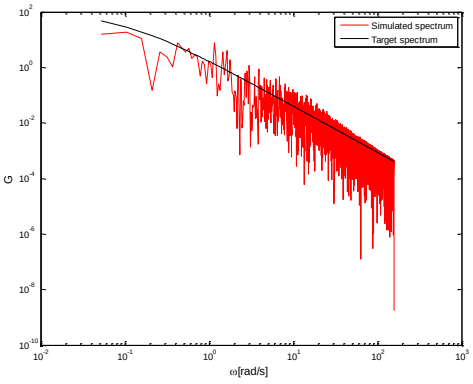

(a) in the horizontal direction

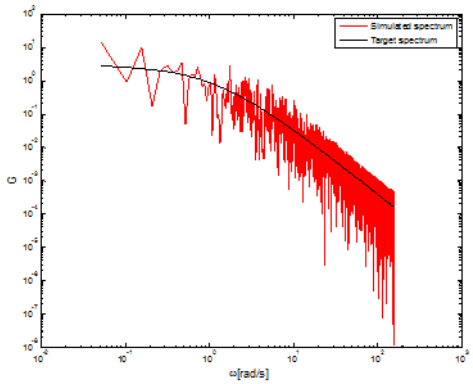

(b) in the vertical direction

Fig. 15 Comparison between the simulated and the target spectrums

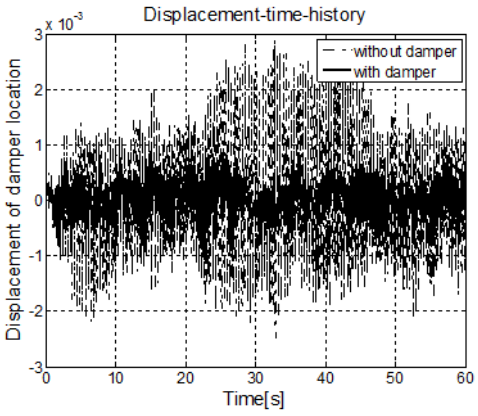

Damper location

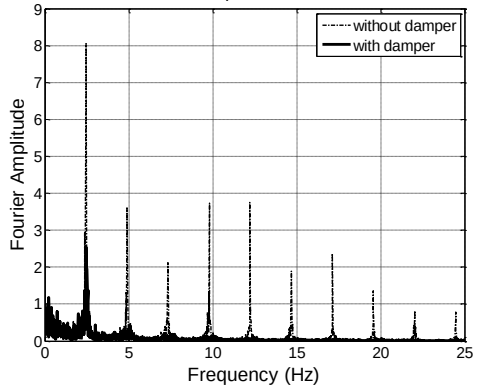

(a) at damper location

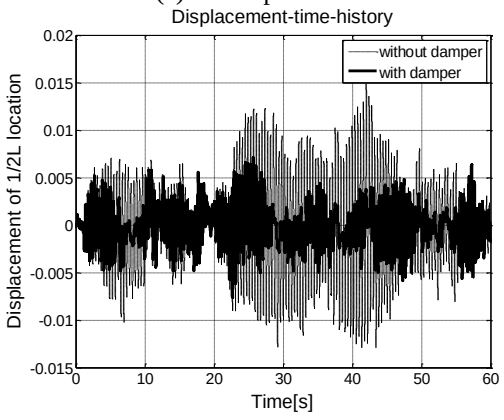

1/2L location

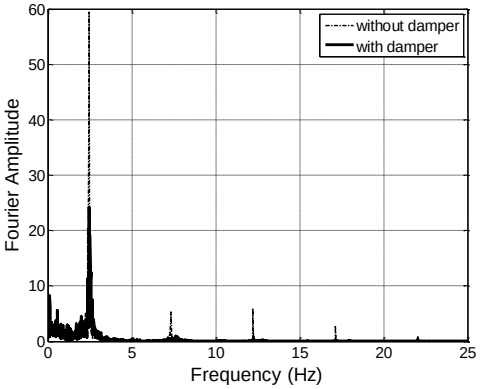

(b) at Mid-span

Continued-

Table 9 Comparison of the RMS value of the displacement responses under wind induced vibration

Control measure	Damper location		1/2L location		1/4L location	
	σ_{rms}	Reduction rate	σ_{rms}	Reduction rate	σ_{rms}	Reduction rate
w/o D	0.8536	--	4.9711	--	3.6974	--
w D	0.3139	63.23	2.2672	54.38	1.5719	57.48

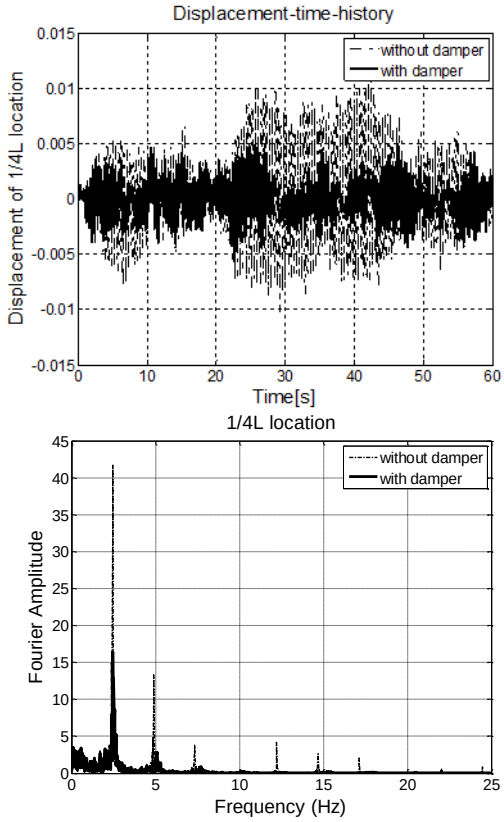

(c) at 1/4*L* location

Fig. 16 Time history and power spectrum of displacement response

The performance of the MR damper can also be shown by comparing the RMS value of the displacement responses, before and after installing the optimally tuned MR damper, as summarized in Table 9. It shows that with the installation of MR damper, the vibration of the cable was significantly reduced. The reduction rate is about 63.23% at the damper location, 54.38% at the mid-span, and 57.48% at the 1/4L of the cable.

The results in this session proved that in the case of cable vibration induced by buffeting wind loads, mainly lower and single mode of vibration was excited at the mid-span of the cable, while at the damper location, multi modes of vibration were generated. All these vibrations can be well suppressed using the proposed optimal control strategy with MR damper.

4. Conclusions

This paper investigated the problem of mitigating multi-mode cable vibrations which was often observed in the field. MR damper was proposed as the control device because of its semi-active feature, where its parameters can be changed by an active control algorithm without requiring large power resources. Because both physical models of cable and MR damper are nonlinear, it is hard to design an efficient and easily adapted control strategy. Therefore, this paper aims to overcome the difficulties in nonlinear modeling and improve the control performance of MR damper, especially for multi-mode cable vibration control. An innovative but simple control algorithm was derived, where the universal design curve of friction dampers was first used to obtain the desired optimal damper force, and then the input voltage (current) of MR damper corresponding to the desired optimal damper was determined using a piecewise linear interpolation scheme from the nonlinear Bouc-wen model of the damper. The effectiveness of the proposed control algorithm was validated through a series of numerical simulations where multi-mode cable vibrations were induced by different loading scenarios such as sinusoidal excitations, white noise excitations and wind loads.

All the simulation results proved that the proposed optimal control strategy using MR damper can effectively mitigate multi-mode cable vibrations of different types, namely, vibrations containing merely lower modes, vibrations involving both lower and higher modes, and vibrations induced by wind loads. Also, as the MR damper was tuned to work as an optimal friction damper, its effectiveness does not depend on the mode of vibration but rather on the amplitude of vibration. Hence, the proposed control strategy using MR damper is especially suitable for controlling multi-mode cable vibrations.

Acknowledgments

This research is supported by the Ministry of Science and Technology of China, Grant No. SLDRCE14-B-25.

References

Chen, Z.Q., Wang, X.Y., Ko, J.M., Ni, Y.Q., Spencer, B.F., Jr., Yang, G. and Hu, J.H. (2004), "MR damping system for mitigating wind-rain induced vibration on Dongting Lake Cable-Stayed Bridge", *Wind Struct.*, **7**(5), 293-304. http://dx.doi.org/10.12989/was.2004.7.5.293.

Duan, Y.F., Ni, Y.Q. and Ko, J.M. (2005), "State-derivative feedback control of cable vibration using semi-active MR dampers", *Comput.-Aided Civil Infrastruct. Eng.*, **20**(6), 431-449. https://doi.org/10.1111/j.1467-8667.2005.00396.x.

Duan, Y.F., Ni, Y.Q. and Ko, J.M. (2006), "Cable vibration control using Magneto-rheological (MR) dampers", *J. Intel. Mat. Syst. Struct.*, **17**(4), 321-325. https://doi.org/10.1142/9789812702197_0121.

Duan, Y.F., Ni, Y.Q., Zhang, H.M., Spencer, B.F., Jr. and Ko, J.M. (2019a), "Design formulas for vibration control of taut cables using passive MR dampers", *Smart Struct. Syst*., Accepted.

Duan, Y.F., Ni, Y.Q., Zhang, H.M., Spencer, B.F., Jr. and Ko, J.M. (2019b), "Design formulas for vibration control of sagged cables using passive MR dampers", *Smart Struct. Syst*., Accepted.

Duan, Y.F., Tao, J.J., Zhang, H.M., Wang, S.M. and Yun, C.B. (2018), "Real-time hybrid simulation based on vector form intrinsic finite element and field programmable gate array", *Struct. Control Health Monit.*, e2277; https://doi.org/10.1002/stc.2277.

Huang, H.W, Liu, J.Y, and Sun, L.M. (2015), "Full-scale experimental verification on the vibration control of stay cable using optimally tuned MR damper", *Smart Struct. Syst*., **16**(6), 1003-1021. http://dx.doi.org/10.12989/sss.2015.16.6.1003.

Huang, H.W., Sun, L.M. and Jiang, X.L. (2012), "Vibration mitigation of stay cable using optimally tuned MR damper", *Smart Struct. Syst*., **9**(1), 35-53. http://dx.doi.org/10.12989/sss.2012.9.1.035.

Johnson, E.A., Baker, G.A., Spencer, Jr. B.F. and Fujino, Y. (2007), "Semiactive damping of stay cables", *J. Eng. Mech. -ASCE*, **133**(1), 1-11. https://doi.org/10.1061/(ASCE)0733-9399(2007)133:1(1).

Krenk, S. (2000), "Vibration of a taut cable with an external damper", *J. Appl. Mech. -T ASME*, **67**(4), 772-776. doi:10.1115/1.1322037.

Liu, J.Y., Huang, H.W. and Sun, L.M. (2013), "Simulation study of semi-active control of stay cable using MR damper under wind loads", *Proc. of SPIE: Smart Structures and Materials & NDE and Health Monitoring 2013*, San Diego, California, USA.

Lu, L., Duan, Y.F., Spencer, B.F. Jr., Lu, X.L. and Zhou, Y. (2017), "Inertial mass damper for mitigating cable vibration", *Struct. Control Health Monit.*, **24**, e1986, doi: 10.1002/stc.1986.

Main, J.A. and Jones, N.P. (2002a), "Free vibrations of taut cable with attached damper I: linear viscous damper", *J. Eng. Mech. -ASCE*, **128**(10), 1062-1071. https://doi.org/10.1061/(ASCE)0733-9399(2002)128:10(1062).

Main, J.A. and Jones, N.P. (2002b), "Free vibrations of taut cable with attached damper I: nonlinear viscous damper", *J. Eng. Mech. -ASCE*, **128**(10), 1072-1081. https://doi.org/10.1061/(ASCE)0733-9399(2002)128:10(1072).

Or, S.W., Duan, Y.F., Ni, Y.Q., Chen, Z.H. and Lam, K.H. (2008). "Development of Magnetorheological dampers with embedded piezoelectric force sensors for structural vibration control", *J. Intel. Mat. Syst. Struct.*, **19**(11), 1327-1338. https://doi.org/10.1177/1045389X07085673.

Pacheco, B.M, Fujino, Y. and Sulekh, A. (1993), "Estimation curve for modal damping in stay cables with viscous damper", *J. Eng. Mech. -ASCE*, **119**(6), 1961-1979. https://doi.org/10.1061/(ASCE)0733-9445(1993)119:6(1961).

Spencer, B.F., Jr., Dyke, S.J, Sain, M.K. and Carlson, J.D. (1997), "Phenomenological model for magnetorheological dampers", *J. Eng. Mech. -ASCE*, **123**(3), 230-238. https://doi.org/10.1061/(ASCE)0733-9399(1997)123:3(230).

Sun, L.M., Shi, C. and Zhou, H.J. (2004), "Parameter optimization of stay cable damper with fractional damping and stiffness", *Proceedings of the 2nd International Conference on Structural Engineering, Mechanics and Computation*, Cape Town, South Africa.

Tabatabai, H. and Mehrabi, A.B. (2000), "Design of viscous dampers for stay cables", *J. Bridge Eng. -ASCE*, 114-123.

Wang, H.P. and Sun, L.M. (2013), "Semi-active control of stay cables using nonlinear friction damper", *Proceedings of SPIE Conference on Sensors and Smart Structures Technologies for Civil, Mechanical, and Aerospace Systems*, San Diego, California, USA.

Wang, X.Y., Ni, Y.Q., Ko, J.M. and Chen, Z.Q. (2005), "Optimal design of viscous dampers for multi-mode vibration control of bridge cables", *Eng. Struct*., **27**(5), 792-800. https://doi.org/10.1016/j.engstruct.2004.12.013.

Weber, F. (2013), "Bouc-Wen model-based real-time force tracking scheme for MR dampers", *Smart Mater. Struct*., **22**(4), 45012-45023.

Weber, F., Feltrin, G., Maślanka, M., Fobo, W. and Distl, H. (2009), "Design of viscous dampers targeting multiple cable modes", *Eng. Struct.*, **31**(11), 2797-2800. https://doi.org/10.1016/j.engstruct.2009.06.020.

Weber, F., Hogsberg, J. and Krenk, S. (2010), "Optimal tuning of amplitude proportional Coulomb friction damper for maximum cable damping", *J. Struct. Eng. -ASCE*, **136**(2), 123-134. https://doi.org/10.1061/(ASCE)0733-9445(2010)136:2(123).

Ying, Z.G., Ni, Y Q. and Ko, J.M. (2007), "Parametrically excited instability analysis of a semi-actively controlled cable", *Eng. Struct.*, **29**(4), 567-575. https://doi.org/10.1016/j.engstruct.2006.05.020.